5th International Conference
"Computational Mechanics and Virtual Engineering"
COMEC 2013
24- 25 October 2013, Braşov, Romania

ON THE SONIC COMPOSITES WITH DEFECTS

Iulian Girip[1], Rodica Ioan[1, 2], Mihaela Alexandra Popescu[1], Ligia Munteanu[1], Veturia Chiroiu[1]
[1]Institute of Solid Mechanics, Bucharest,
[2]University Spiru Haret, Bucharest

Dedicated to the memory of Prof. Petre P. Teodorescu (1929-2013).

Abstract: *The sound attenuation in a sonic composite with point defects is studied using a new method that combines the features of the cnoidal method and the genetic algorithm. Acoustic scatterers are composed by piezoceramic hollow spheres of functionally graded materials - the Reddy and cosine graded hollow spheres. This method enables to obtain the dispersion relation for defect modes, and the prediction of the evanescent nature of the modes inside the band-gaps.*
Key-Words: *Sonic composites, sound attenuation, defects, evanescent waves, full band-gaps.*

1. INTRODUCTION

A sonic composite is a finite size periodic array composed of scatterers embedded in a homogeneous material [1-3]. A great number of applications based on the sonic composites are explained by the existence of the band-gaps into the acoustic filters, acoustic barriers or wave guides [4-7]. The generation of large band-gaps is due to the superposition of multiple reflected waves within the array according to the Bragg's theory, and consequently, it is connected with a large acoustic impedance ratio between the scatterers' material and the matrix' material, respectively.
The band-gaps correspond to the Bragg reflections that occur at different frequencies inverse proportional to the central distance between two scaterers. The waves are reflected completely from this periodic array in the frequency range where all partial band-gaps for the different periodical directions overlap. This makes sharp bends of the wave-guide in the sonic composite. The evanescent waves characterized by complex wave numbers, are distributed across the boundary of the waveguide into the surrounding composite by several times the lattice constant [8].
Recent experimental and theoretical results [9-11] show that the presence of defects in sonic composite is related to the generation of localized modes in the vicinity of the point defect with a significant evanescent behavior of the waves outside the defect point. This means that the evanescent modes are related to the existence of the band-gaps where no real wave number exists. The authors have revealed that the level of the sound is higher inside the vicinity of the defect point than into the composite. Recent works show the calculation of complex band structures for photonic crystals [12-14], using the explicit matrix formulation and the approximation of the supercells. This technique enables to be extended to the 2D complete sonic composites, as well as in sonic composites with point defects.
The goal of this paper is to propose an alternative method for obtaining the band structures of the 3D sonic composites without/ with point defects. The point defects are vacancies or foreign interstitial atoms which are supported by the interfaces between the hollow spheres and the matrix. The proposed method is used to simulate a sonic plate composed of an array of acoustic scatterers which are piezoceramic hollow spheres embedded in an epoxy matrix. The scatterers are made from functionally graded materials with radial polarization, which support the Reddy and cosine laws [15-17]. Readers are also referred to [18-20] for vibrations of solid spheres of functionally graded materials and for the wave propagation in functionally graded materials.
The proposed approach is based on the theory of piezoelectrics coupled with the cnoidal method and a genetic algorithm. For a single sphere made from a functionally graded material, the free vibration problem was analyzed in [21-25].

2. THEORY

The sonic composite is consisting of an array of acoustic scatterers embedded in an epoxy matrix. The acoustic scatterers are hollow spheres made from a nonlinear isotropic piezoelectric ceramic, while the matrix is made from a nonlinear isotropic epoxy resin (Figure 1). The sonic plate consists of 72 local resonators of diameter a. A rectangular coordinate system $Ox_1x_2x_3$ is employed. The origin of the coordinate system $Ox_1x_2x_3$ is located at the left end, in the middle plane of the sample, with the axis Ox_1 in-plane and normal to the layers and the axis Ox_3 out-plane and normal to the plate. The length of the plate is l, its width is d, while the diameter of the hollow sphere is a and its thickness is $e > a$. In order to avoid unphysical reflections from the boundaries of the specimen, we have implemented the absorbing boundary conditions in the x_1-direction, at $x_1 = 0$ and $x_1 = l$. A transducer and a receiver are located at $x_1 = b$ and $x_1 = l - b$, respectively. The role of the transducer is to inject into the plate the plane monochromatic waves propagating in the x_1-direction.

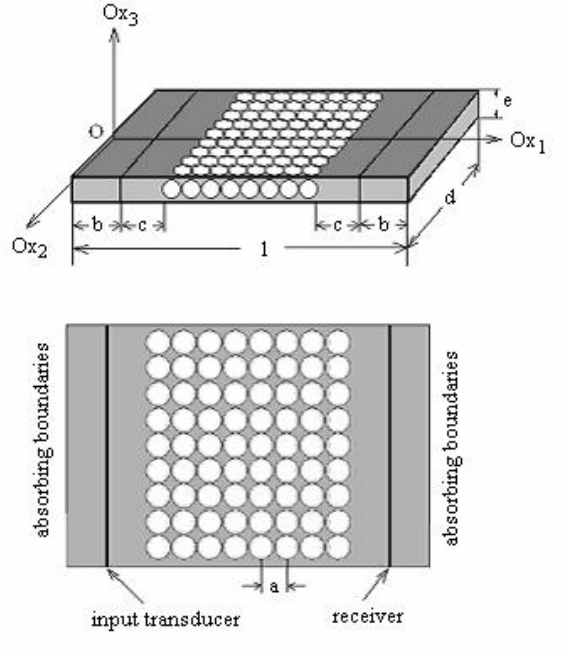

Figure 1: Sketch of the sonic composite.

The governing equations are given by [2, 3]

$rA_{,r} = MA$, $rB_{,r} = PB$, (1)

where

$B = [\Sigma_{rr}, \Sigma_2, G, w, \Lambda_r, \phi]^T$,

$$M = \begin{bmatrix} -2 & -C_{66}(\nabla^2 + 2) + r^2 \rho \dfrac{\partial^2}{\partial t^2} \\ C_{44}^{-1} & 1 \end{bmatrix},$$

with $\nabla^2 = \dfrac{\partial^2}{\partial \theta^2} + \cot\theta \dfrac{\partial}{\partial \theta} + \csc^2\theta \dfrac{\partial^2}{\partial \varphi^2}$. It should be noted that equation $(1)_1$ is related to two state variables, namely $A = [\Sigma_1, F]^T$, while equations $(1)_2$ are related to six state variables $\Sigma_{rr}, \Sigma_2, G, w, \Lambda_r, \phi$

$\Sigma_{rr} = r\sigma_{rr} = C_{13}S_{\theta\theta} + C_{13}S_{\varphi\varphi} + C_{33}S_{rr} + f_{33}r\phi_{,r}$

$\Lambda_r = rD_r = f_{31}S_{\theta\theta} + f_{31}S_{\varphi\varphi} + f_{33}S_{rr} - \zeta_{33}r\phi_{,r}$,

$u_\theta = -\csc\theta F_{,\varphi} - G_{,\theta}$, $u_\varphi = F_{,\theta} - \csc\theta G_{,\varphi}$, $u_r = w$,

$\Sigma_{r\theta} = -\csc\theta\Sigma_{1,\varphi} - \Sigma_{2,\theta}$, $\Sigma_{r\varphi} = \Sigma_{1,\theta} - \csc\theta\Sigma_{2,\varphi}$. (2)

where σ_{ij} is the stress tensor, ϕ is the electric potential, D_i is the electric displacement vector, C_{ij} are the elastic constants, $C_{66} = (C_{11} - C_{12})/2$, f_{ij} are the piezoelectric constants f_{ij}, ζ_{ij} are the dielectric constants, and

$i = r, \theta, \varphi$. The elastic, piezoelectric and dielectric constants are arbitrary functions of the radial coordinate r . On denoting the components of the strain tensor and displacement vector by ε_{ij} and u_i , $i = r, \theta, \varphi$, respectively. The nonzero components of the matrix P are given by

$$P_{11} = 2\beta - 1,\ P_{12} = \nabla^2,\ P_{13} = k_1\nabla^2,\ P_{14} = -2k_1 + r^2\rho\frac{\partial^2}{\partial t^2},$$

$$P_{15} = 2P_{25} = -P_{64} = 2\gamma,\ P_{21} = \beta,\ P_{22} = -2,\ P_{23} = k_2\nabla^2 - 2C_{66} + r^2\rho\frac{\partial^2}{\partial t^2},$$

$$P_{24} = -k_1,\ P_{32} = C_{44}^{-1},\ P_{33} = P_{34} = -P_{55} = 1,\ P_{36} = C_{44}^{-1}f_{15},\ P_{41} = \alpha^{-1}\zeta_{33},\ P_{43} = \beta\nabla^2,$$

$$P_{44} = -2\beta,\ P_{45} = \alpha^{-1}f_{33},\ P_{52} = C_{44}^{-2}f_{15}\nabla^2,\ P_{56} = k_3\nabla^2,\ P_{61} = \alpha^{-1}f_{33},\ P_{63} = \gamma\nabla^2,\ P_{65} = -\alpha^{-1}C_{33}, \quad (3)$$

where

$$\alpha = C_{33}\zeta_{33} + f_{33}^2,\ \beta = \alpha^{-1}(C_{13}\zeta_{33} + f_{31}f_{33}),\ \gamma = \alpha^{-1}(C_{13}f_{33} - C_{33}f_{31}),$$

$$k_1 = 2(C_{13}\beta + f_{31}\gamma) - (C_{11} + C_{12}),\ k_2 = 0.5k_1 - C_{66},\ k_3 = \zeta_{11} + f_{15}^2C_{44}^{-1}.$$

Consider now two piezoceramic hollow spheres with the ratio of the inner and outer radii ξ_0 . Two laws represent the functionally graded property of the material. The first one is the Reddy law given by [15-17]

$$M = M_p\mu^{\lambda} + M_z(1 - \mu^{\lambda}), \quad (4)$$

where μ is the gradient index [22], M_p and M_z are material constants of two materials, namely PZT-4 and ZnO. The case $\mu = 0$ corresponds to a homogeneous PZT-4 hollow sphere and $\mu \to \infty$, to a homogeneous ZnO hollow sphere. The second law is expressed as

$$M = M_p\cos\mu + M_z(1 - \cos\mu). \quad (5)$$

At the interfaces between the hollow spheres and the matrix, sharp periodic boundary conditions for the displacement and traction vectors are added [29] for sonic composites without/with defects. In addition, in the case of the point defects situated in the interfaces between the hollow spheres and the matrix, a new equation must be added to reflect the dynamic of the concentration of the defects.

The distribution of the defects of the concentration $c(r)$ is characterized by the diffusive contribution $-D\nabla c$, where D is the diffusion coefficient, and the forced contribution ηcF where η is the mobility and F the driving force which acts upon the defects. The mobility and the diffusivity are related through the Nernst-Einstein relation $D = \eta kT$ where k is the Boltzmann's constant and T the absolute temperature.

The rate of the change of the concentration in the presence of the source $S(r,t)$ is [26]

$$\frac{\partial c}{\partial t} = -\nabla\left(-D\nabla c\right) + S(r,t), \quad (6)$$

or

$$\frac{\partial c}{\partial t} = D\left(\nabla^2 c - \frac{1}{kT}\left(F\nabla c + c\nabla F\right)\right) + S(r,t). \quad (7)$$

The source $S(r,t)$ represents the rate at which the defects are created at any point.

3. THE BEHAVIOR OF THE SONIC COMPOSITE WITH DEFECTS

Consider a plate with the length $l = 18\text{cm}$ and width $d = 11\text{cm}$, while the diameter of the hollow sphere and its thickness are $a = 10.5\text{mm}$ and $e = 12\text{mm}$, respectively, and $\xi_0 = 0.3$. The numerical results are carried out for the following constants [2]:

for PZT-4 $C_{11} = 13.9\times10^{10}\,\text{N/m}^2$, $C_{12} = 7.8\times10^{10}\,\text{N/m}^2$, $C_{13} = 7.4\times10^{10}\,\text{N/m}^2$,

$C_{33} = 11.5\times10^{10}\,\text{N/m}^2$, $C_{44} = 2.56\times10^{10}\,\text{N/m}^2$, $f_{15} = 12.7\text{C/m}^2$, $f_{31} = -5.2\text{C/m}^2$,

$f_{33} = 15.1\text{C/m}^2$, $\zeta_{11} = 650\times10^{-11}\,\text{F/m}$, $\zeta_{33} = 560\times10^{-11}\,\text{F/m}$, $\rho = 7500\text{kg/m}^3$,

for ZnO $C_{11} = 20.97\times10^{10}\,\text{N/m}^2$, $C_{12} = 12.11\times10^{10}\,\text{N/m}^2$, $C_{13} = 10.51\times10^{10}\,\text{N/m}^2$,

$C_{33} = 21.09\times10^{10}\,\text{N/m}^2$, $C_{44} = 4.25\times10^{10}\,\text{N/m}^2$, $f_{15} = -0.59\text{C/m}^2$, $f_{31} = -0.61\text{C/m}^2$,

$f_{33} = 1.14\text{C/m}^2$, $\zeta_{11} = 7.38\times10^{-11}\,\text{F/m}$, $\zeta_{33} = 7.83\times10^{-11}\,\text{F/m}$, $\rho = 5676\text{kg/m}^3$,

and for epoxy-resin $\lambda^e = 42.31\times10^9\,\text{N/m}^2$, $\mu^e = 3.76\times10^9\,\text{N/m}^2$, $A^e = 2.8\times10^9\,\text{N/m}^2$, $B^e = 9.7\times10^9\,\text{N/m}^2$,

$C^e = -5.7\times10^9\,\text{N/m}^2$, and $\rho^e = 1170\,\text{kg/m}^3$.

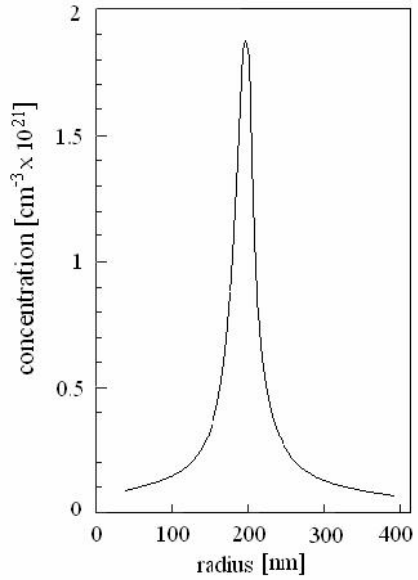

Figure 2: Variation of the concentration with respect to the radius of Σ which encloses the point defect.

The independent sets of equations (1) yield two independent classes of free vibrations. The first class does not involve the piezoelectric or dielectric parameters, being identical to the one for the corresponding spherically isotropic elastic sphere. The second class depends on the piezoelectric or dielectric parameters. With the increase of the gradient index μ, the natural frequencies increase for all modes and functionally graded laws, the variation being more significant when $\mu \le 10$. For $\mu \to \infty$ the variation of natural frequencies is not significant with respect to those of $\mu = 10$. It is seen that for a piezoceramic hollow sphere, the piezoelectric effect consists of increasing the values for the natural frequencies in both classes of vibrations. If $\xi = 2r/a$ increases, the natural frequencies increase for the first class of vibrations and decrease for the second class.

The propagation of sound is characterized by the superposition of multiply reflected waves. Featuring of the length scale a, the structure of the full band-gap can be better understood by representing the linear band structure (dispersion curve).

The simulation is carried out for a variation of the defects concentration represented in Figure 2 with respect to the radius of Σ which encloses the point defect (vacancies or foreign interstitial atoms), for 300K. In this figure only the effect of diffusion is shown, without any stress gradient, after 1000sec.

Figure 3 plots the dispersion curve including the first partial band-gaps for the composite without defects and for the composite with defects ($c = 1.5 \times 10^{21}\,\mathrm{cm}^{-3}$). The reduced units for the frequency are $\omega a / 2\pi c_0$, with c_0 the speed of sound in air. We see that the point defects confine acoustic waves in localized modes and in consequence the band-gaps are larger than in the case of the complete composite.

The guided waves are accompanied by evanescent waves which extend to the periodic array of the scatterers surrounding the wave-guide. Using the Joannopoulus representation [8] for the bad-gap structure, Figure 4 presents the band structure with the evanescent modes with exponential decay for the sonic composite without defects. The modes present purely imaginary wave vectors. The central grey region is the full band-gap ranged between 8.02 kHz and 8.72 kHz, given by the real part of the wave vector constrained in the first Brillouin zone for each frequency. The left region represents the imaginary part of the wave vector for longitudinal direction frequency (tension/compression), while the right region is the imaginary part of the wave vector for transverse direction frequency (shear). The red lines represent the imaginary part of the wave vector of the evanescent modes inside the bad-gap.

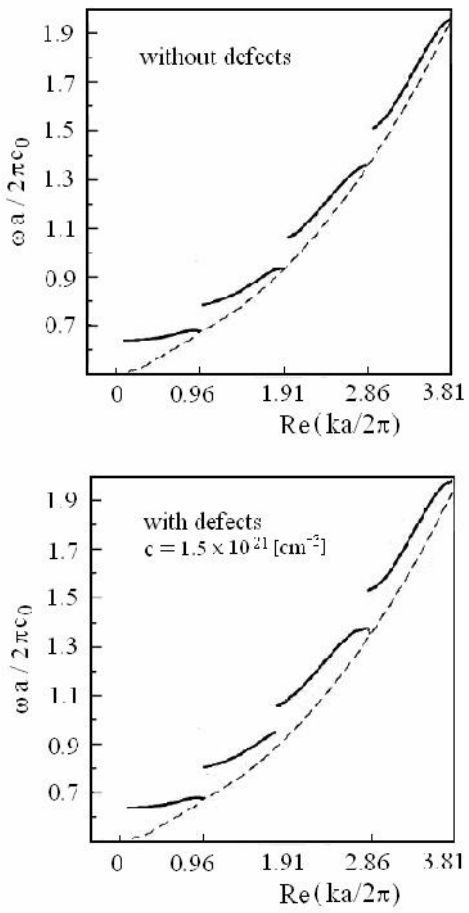

Figure 3: Linear dispersion for sonic composite without/with defects.

If we want to have a full band-gap, we must have structures with band-gaps for both longitudinal and transverse waves in the same frequency region.
The difference in the sound velocities between transverse and longitudinal modes causes partial gaps at different frequencies. If the mechanical contrast is small, these partial gaps are narrow and do not overlap. As mechanical contrast increases, the partial gaps widen and begin to overlap in the same frequency region leading to the appearance of a full band-gap independent of the polarization.

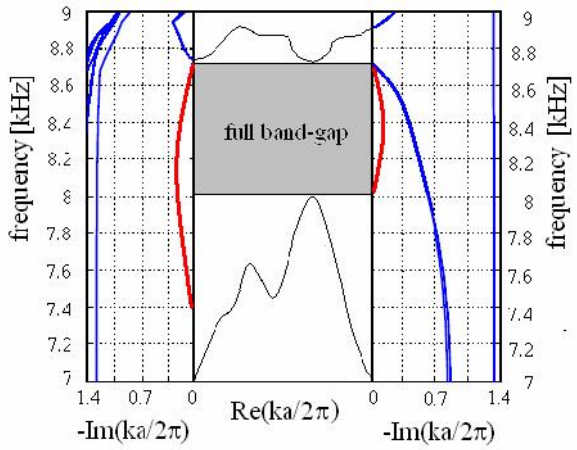

Figure 4: Band structure for the sonic composite without defects in the case of Reddy law.

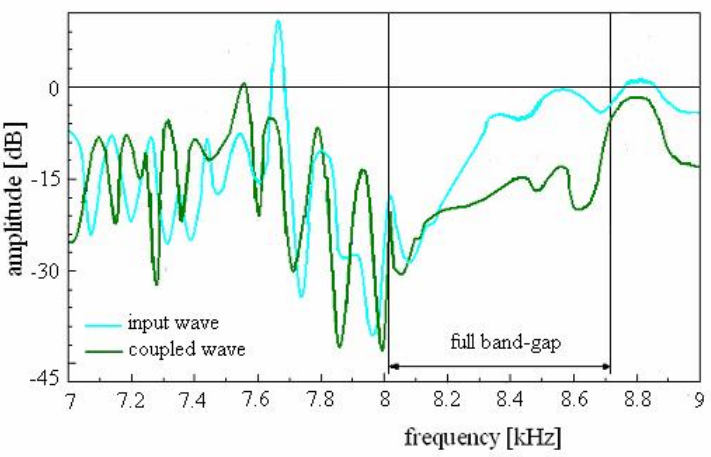

Figure 5 : The input and coupled waves for sonic composite without defects in the case of Reddy law.

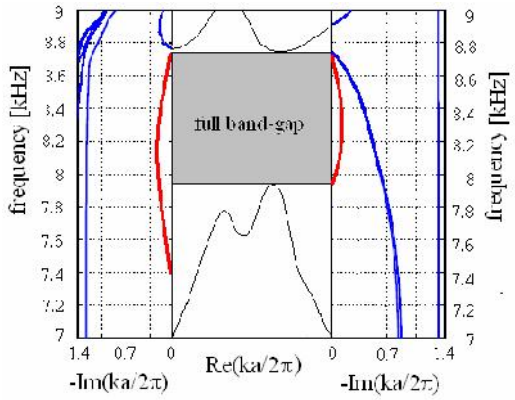

Figure 6: Band structure for the sonic composite with defects ($c = 1.5 \times 10^{21}\,\mathrm{cm}^{-3}$) in the case of Reddy law.

It is strongly expected that mode coupling waves arise between adjacent wave-guides. The output of the coupled modes is compared with the input waves, as shown in Figure 5 in the case of Reddy law and $\sigma_e = 2.2\mathrm{kPasm}^{-2}$. Figure 6 presents the band structure for the sonic composite with defects ($c = 1.5 \times 10^{21}\,\mathrm{cm}^{-3}$) in the case of the Reddy law. We observe that this time the portion widens from 7.95 kHz to 8.76 kHz. The coupled and the input waves are shown in Figure 7 for $\sigma_e = 2.2\mathrm{kPasm}^{-2}$. The difference from the composite without defects consists only in the size and structure of the full band-gaps.

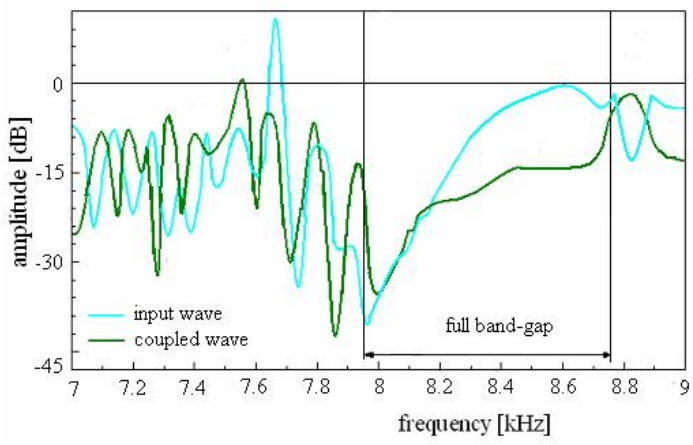

Figure 7 : The input and coupled waves for sonic composite with defects ($c = 1.5 \times 10^{21}\,\mathrm{cm}^{-3}$) in the case of Reddy law.

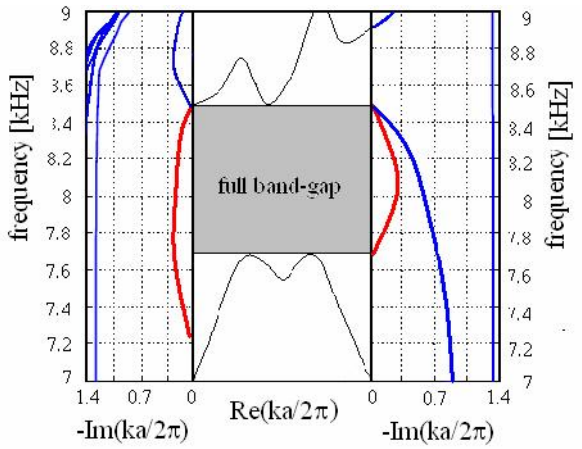

Figure 8: Band structure for the sonic composite with defects ($c = 1.5 \times 10^{21}\,\mathrm{cm}^{-3}$) in the case of the cosine law.

Figure 8 presents the band structure for the sonic composite with defects ($c = 1.5 \times 10^{21}\,\mathrm{cm}^{-3}$) in the case of the cosine law. We observe that the full band-gap has the same length but has undergone a translation, i.e. to 7.67 kHz and 8.48 kHz.
The length of the full band-gap as function of the concentration of the point defects is represented in Figure 9, for both Reddy law and cosine law, respectively. For Reddy law, the length increases with concentration and shows a flat portion starting to the concentration of 1.5 with a slight decrease of concentration at around 0.88 kHz. For the cosine law, the length shows two flat zones and a visible drop of concentration around 0.64 kHz.

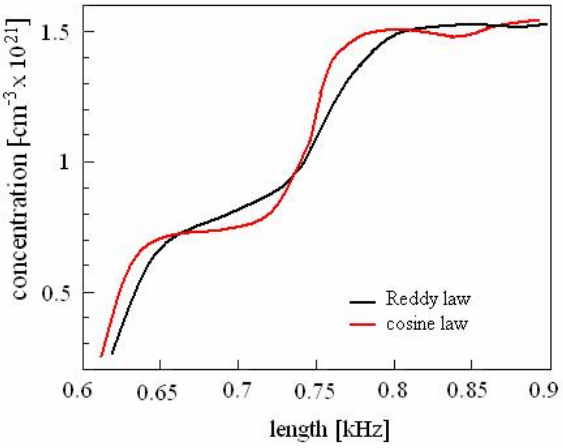

Figure 9: The length of the full band-gap as function of the concentration of the point defects.

6. Conclusions

Analytical and numerical solutions and verification to real results are presented in this paper for propagation of waves in sonic composites without/with defects. The point defects are vacancies or foreign interstitial atoms which are situated in the interfaces between the hollow spheres and the matrix. It is shown that the point defects confine acoustic waves in localized modes, and the defect modes are created within the band-gaps of the composite. The localization of the sound in the defect regions leads to increase in the intensity of the acoustic wave's interactions. Such localizations increase the length of the full band-gap frequency for sonic composites with defects by 15-20% compared with the values for similar composites without defects.
The scattering problem inside the sonic composite is solved by a method which combines the cnoidal method with a genetic algorithm. The reason for choosing the cnoidal method lies in the facts that the governing equations are reduced to Weierstrass equations with polynomials of higher-order, for a change of variable $t \to x - ct$, with c a constant. The solutions are expressed as a sum of the linear and the nonlinear superposition of cnoidal vibrations, respectively

ACKNOWLEDGEMENT.

The authors gratefully acknowledge the financial support of the National Authority for Scientific Research ANCS/UEFISCDI through the project PN-II-ID-PCE-2012-4-0023, Contract nr.3/2013.

REFERENCES

[1] M. Hirsekorn, P.P. Delsanto, N.K. Batra, P. Matic, *Modelling and simulation of acoustic wave propagation in locally resonant sonic materials*, Ultrasonics, 42, 231–235, 2004.
[2] L. Munteanu, V. Chiroiu, *On the dynamics of locally resonant sonic composites*, European Journal of Mechanics-A/Solids, 29(5), 871–878, 2010.
[3] L. Munteanu, *Nanocomposites* , editura Academiei, Bucharest, 2012.
[4] J.V. Sánchez-Pérez, D. Caballero, R. Mártinez-Sala, C. Rubio, J. Sánchez-Dehesa, F. Meseguer, J. Llinares, F. Gálvez, *Sound attenuation by a two-dimensional array of rigid cylinders*, Phys. Rev. Lett. 80(24), 5325-5328, 1998.
[5] J.V. Sánchez-Pérez, C. Rubio, R. Martínez-Sala, R. Sánchez-Grandia, V. Gómez, *Acoustic barrier based on periodic arrays of scatterers*, Appl. Phys. Lett. 81, 5240-5242, 2002.
[6] A. Khelif, A. Choujaa, B. Djafari-Rouhani, M. Wilm, S. Ballandras, V. Laude, *Trapping and guiding of acoustic waves by defect modes in a full-band-gap ultrasonic crystal*, Phys. Rev. B 68, 214301, 2003.
[7] A. Khelif, M. Wilm, V. Laude, S. Ballandras, and B. Djafari-Rouhani, *Guided elastic waves along a rod defect of a two-dimensional photonic crystal,* Phys. Rev. E 69(6), 067601, 2004.
[8] J.D. Joannopoulus, S.G. Johnson, J.N. Winn, R.D. Meade, *Photonic Crystals. Molding the Flow of Light,* Princeton University Press, 2008.
[9] V. Romero-García, J.V. Sánchez-Pérez, L.M. Garcia-Raffi, *Evanescent modes in sonic crystals: Complex relation dispersion and supercell approximation*, Journal of Applied Physics, 108(4), 108-113, 2010.
[10] F. Wu, Z. Hou, Z. Liu, T. Liu, *Point defect states in two-dimensional phononic crystals*, Phys. Lett. A 292, 198, 2001.
[11] Y. Zhao, L.B. Yuan, *Characteristics of multi-point defect modes in 2D photonic crystals*, J. Phys. D: Appl. Phys. 42(1), 015403, 2009.
[12] T. Miyashita, *Full band gaps of sonic crystals made of acrylic cylinders in air-numerical and experimental investigations*, Japanese Journal of Applied Physics, 41, 3170-1-3175, 2002.
[13] V. Laude, Y. Achaoui, S. Benchabane, A. Khelif, *Evanescent Bloch waves and the complex band structure of phononic crystals*, Phys. Rev. B 80, 092301 (2009).
[14] R. Sainidou, N. Stefanou, *Guided and quasiguided elastic waves in photonic crystal slabs*, Phys. Rev. B 73, 184301, 2006.
[15] J.N. Reddy, *A Generalization of Two-Dimensional Theories of Laminated Composite Laminate*, Comm. Appl. Numer. Meth., 3, 173–180, 1987.
[16] J.N. Reddy, C.F. Liu, *A higher-order theory for geometrically nonlinear analysis of composite laminates*, NASA Contractor Report 4056, 1987.
[17] J.N. Reddy, C.M. Wang, S. Kitipornchai, *Axisymmetric bending of functionally graded circular and annular plates*, Eur. J. Mech., A/Solids 18, 185–199, 1999.
[18] B.M. Singh, J. Rokne, R.S. Dhaliwal, *Vibrations of a solid sphere or shell of functionally graded materials*, European Journal of Mechanics-A/Solids, 27, 3, 460–468, 2008.
[19] B. Collet, M. Destrade, G.A. Maugin, *Bleustein-Gulyaev waves in some functionally graded materials*, European Journal of Mechanics-A/Solids, 25, 5, 695–706, 2006.
[20] A. Berezovski, J. Engelbrecht, G.A. Maugin, *Numerical simulation of two-dimensional wave propagation in functionally graded materials*, European Journal of Mechanics-A/Solids, 22, 2, 257–265, 2003
[21] V. Chiroiu, L. Munteanu, *On the free vibrations of a piezoceramic hollow sphere*, Mech. Res. Comm., Elsevier, 34, 2, 123–129, 2007.
[22] W.Q. Chen, L.Z. Wang, and Y. Lu, *Free vibrations of functionally graded piezoceramic hollow spheres with radial polarization*, J. Sound Vibr., 251, 1, 103–114, 2002.
[23] W. Q. Chen, *Vibration theory of non-homogeneous, spherically isotropic piezoelastic bodies*, J. Sound Vibr., 229, 833–860, 2000.
[24] M. Mihailescu, V. Chiroiu, *Advanced mechanics on shells and intelligent structures,* Editura Academiei, Bucharest, 2004.
[25] R.A. Toupin, *Piezoelectric relations and the radial deformation of a polarized spherical shell*, J. Acoust. Soc. Am., 31, 315–318, 1959.
[26] Britton, D.T., Harting, M., *The influence of strain on point defect dynamics*, Advanced Engineering Materials, 4(8), 628-635, 2008.